Available online at www.sciencedirect.com
SCIENCE DIRECT®
Journal of Power Sources 119–121 (2003) 918–923
JOURNAL OF POWER SOURCES
www.elsevier.com/locate/jpowsour

Self-discharge study of $LiCoO_2$ cathode materials

Yasunori Ozawa, Rachid Yazami*, Brent Fultz

Division of Engineering and Applied Science, California Institute of Technology, Mail code 138-78, Pasadena, CA 91125, USA

Abstract

The time dependence of the open-circuit voltage (OCV) and the capacity loss in $Li/Li_{1-y}CoO_2$ half-cells during high temperature aging were measured experimentally, and tentatively simulated with simple kinetics equations involving Li-ion diffusion and a phase transition, respectively. The respective activation energies were determined. The capacity loss was found to have a reversible and irreversible component. The latter is discussed in contest of recent observation of an irreversible hexagonal-to-spine phase transition.

Keywords: $LiCoO_2$; Temperature effect; Open-circuit voltage; Self-discharge; Activation energy; Spinel

1. Introduction

Lithium-ion batteries dominate the market of power sources for electronic applications due to their high energy and power densities, reliability, long life and safety [1]. However, their behavior after storage at elevated temperature is still not well understood.

Self-discharge is a natural phenomenon in primary and secondary batteries [2]. It originates from different processes within the battery, among them corrosion-type reactions that take place between the electrolyte and electrodes. Lithium-ion batteries in their charged state have a high open-circuit voltage (OCV) close to 4.2 V, which makes it even more likely for the lithiated graphite Li_yC_6 negative (anode) and delithiated positive electrode (cathode) $Li_{1-y}CoO_2$ to be oxidized or reduced by the electrolyte, respectively.

In a recent study on the calendar life of complete lithium-ion prototype cells studied in the floating mode, Broussely et al. [3] found a kinetics law of the type:

$$t = ax^2 + bx, \quad (1)$$

where t is the aging time and x the relative capacity loss. They claim that the origin of the capacity loss is mainly related to the limiting role of the SEI formed on the negative electrode kinetics.

Two-electrode complete cells do not allow us to distinguish clearly between contributions from anode and cathode in capacity loss. Recently, we used lithium/graphite half-cells to study the kinetics and mechanism of capacity loss in the Li_xC_6 electrode side [4]. A first-order kinetics law was found for total capacity loss.

In the present study, we performed similar aging tests with $Li/LiClO_4$ in propylene carbonate (PC)/$Li_{1-y}CoO_2$ half-cells. The cells were cycled between 2.9 and 4.2 V at ambient temperature to determine their initial capacity. They were then stored in their fully-charged state (at initial 4.2 V) at a constant temperature T between 60 and 75 °C for several days while recording their open-circuit voltage. Cells were then first discharged and cycled under the same conditions as before aging, allowing the remaining capacity and the capacity loss to be determined. The average discharge voltages before and after aging were also compared.

The time dependence of the open-circuit voltage and capacity loss fit well with reaction mechanisms involving diffusion and phase transformation.

2. Experimental

$Li/PC\text{-}LiClO_4/LiCoO_2$ coin-type half-cells (CR2016) were used for this study. The cathode, provided by ENAX Inc. (Tokyo, Japan) consists of a composite mixture (91% $LiCoO_2$, 6% graphite and 3% binder) cast on a thin aluminum foil. The separator is made of glass fibers (Craneglas 230/6.1 from Crane Co., New Hyde, NY, USA). The electrolyte is 1 M solution of $LiClO_4$ in propylene carbonate (Mitsubishi Chemicals Co., Tsukuba, Japan). The cells were mounted in dry box filled with argon. They were cycled at ambient temperature at $C/5$ rate between 2.9 and 4.2 V for

* Corresponding author. Present address: LEPMI (INPG-CNRS, UMR 6531), BP 75, 38402 St. Martin d'Hères, France. Tel.: +1-626-395-4496; fax: +1-626-795-6132.
E-mail address: yazami@caltech.edu (R. Yazami).

0378-7753/03/$ – see front matter © 2003 Published by Elsevier Science B.V.
doi:10.1016/S0378-7753(03)00227-1

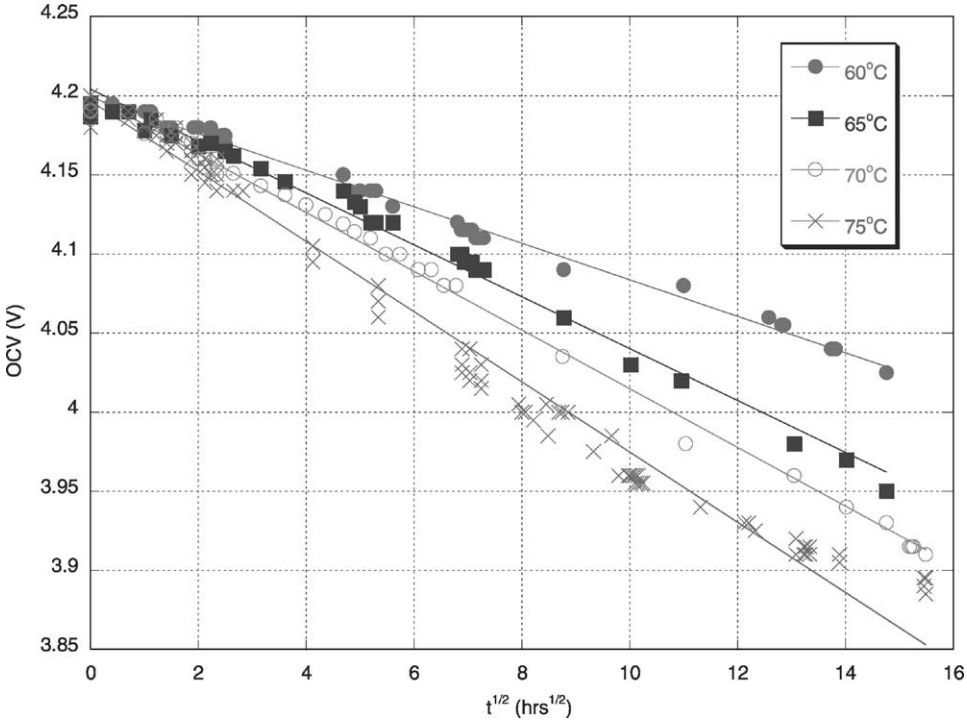

Fig. 1. OCV vs. $t^{1/2}$ curves during aging at 60–75 °C.

several cycles, the final step being a charge to 4.2 V. The cells were then stored at temperatures $T = 60$, 65, 70 and 75 °C for time t between 2 and 10 days. The cell open-circuit voltages $E_0(t, T)$ were monitored during storage. The retained capacity after storage was determined by discharging the cells from their initial OCV to 2.9 V, and their new cycle capacity was determined by applying further cycles between 2.9 and 4.2 V at $C/5$ rate at ambient temperature. X-ray diffraction (XRD) using Co Kα radiation was performed on electrodes before and after aging in their discharged state.

3. Results and discussion

3.1. OCV measurements

The voltage relaxation in single-phase intercalation electrodes is expected to follow a diffusion-controlled

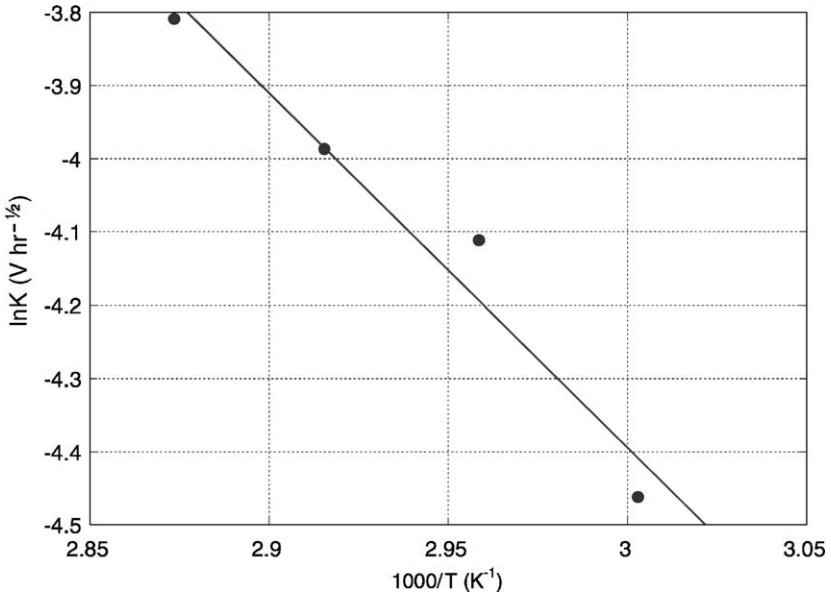

Fig. 2. Arrhenius plot of constant K in Eq. (2).

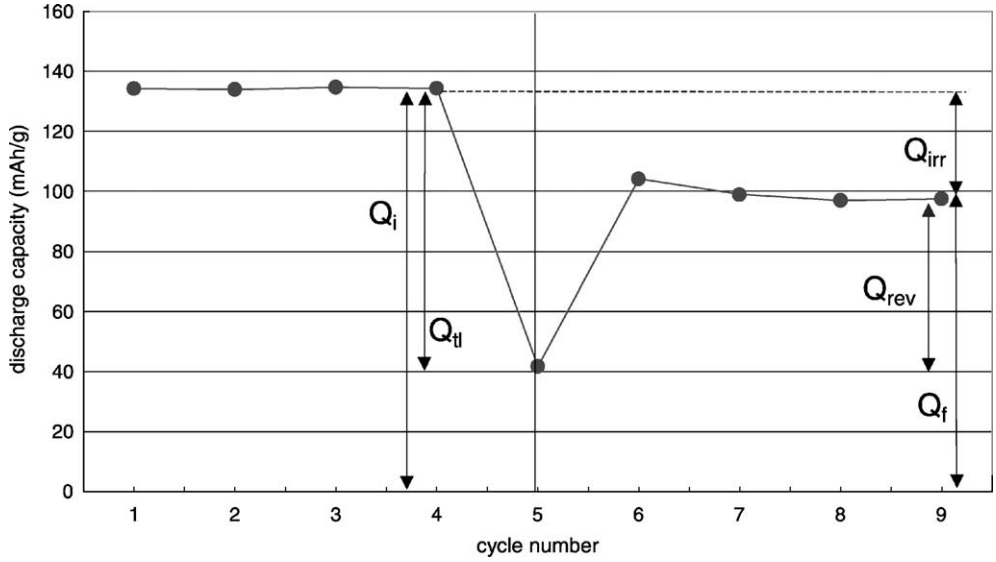

Fig. 3. Schematic representation of the evolution of discharge cycle capacity before and after aging at 75 °C; 10 days.

mechanism. Therefore, a curve fit with a $t^{1/2}$ law was attempted.

Fig. 1 shows the $E_0(t, T)$ versus $t^{1/2}$ transforms. A linear dependence of the type

$$E_0(t, T) = E_0(0, T) - Kt^{1/2}, \quad (2)$$

was found, confirming the diffusion model.

$E_0(t, T)$ relates to the lithium chemical potential at the electrode/electrolyte interface. During thermal aging starting from a delithited state, lithium will diffuse towards empty sites at crystallite boundaries. This will increase the local concentration at the interface, driving the voltage to lower values. A close analysis of the $E_0(t, T)$ versus $t^{1/2}$ curves shows a departure from linearity at higher temperatures and longer storage times. This may suggest other mechanism(s) is/are taking place at the electrode/electrolyte interface. In a recent study by transmission electron microscopy (TEM) [5], direct evidence of the growth of the cubic spinel phase ($Li_{1+y}Co_2O_4$) on the surface of the hexagonal ($Li_{1-y}CoO_2$) was shown. The spinel phase is known to have lower electrochemical activity (i.e. lower discharge voltage and lower capacity) than the hexagonal one [6–9]. The hexagonal → spinel phase transformation is promoted by the delithiation state and by higher temperature [10,11]. Therefore, we do not exclude a contribution from this phase transformation to the open-circuit voltage/time dependence, especially at higher temperature.

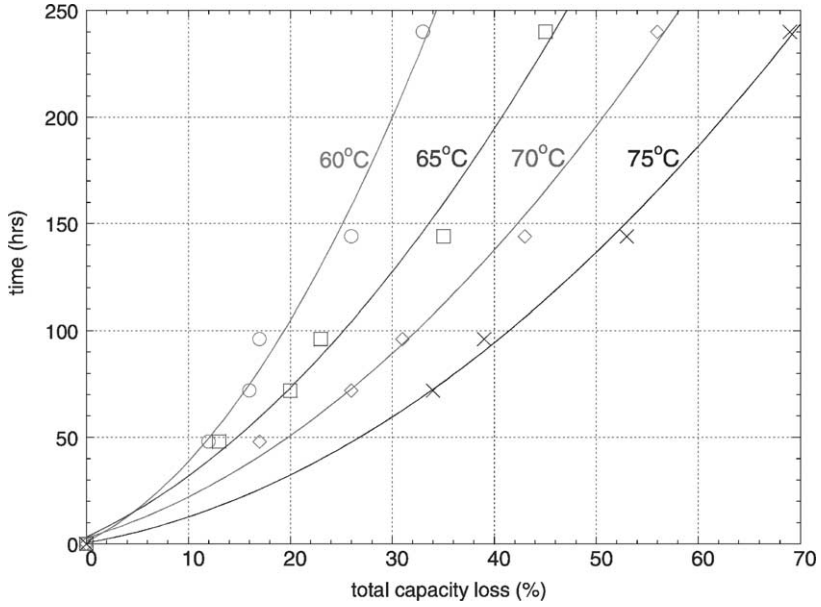

Fig. 4. Time vs. the relative capacity loss at different aging temperatures.

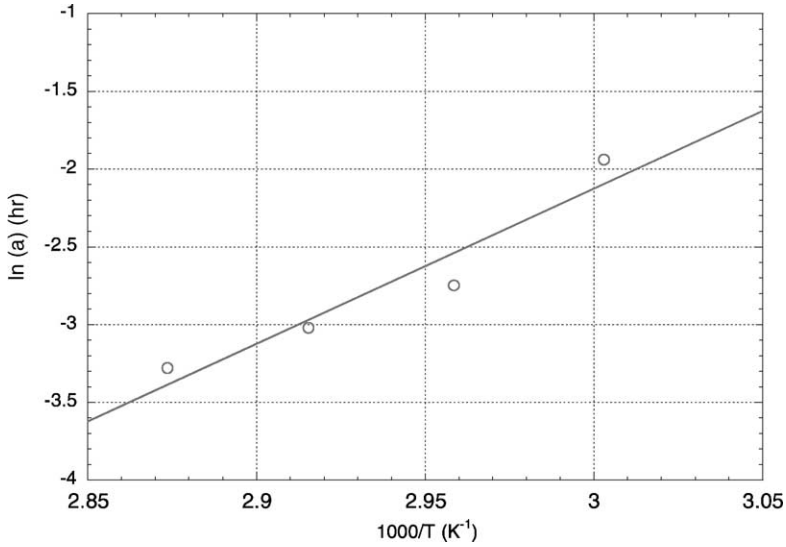

Fig. 5. Arrhenius plot of parameter a in equation $t = ax^2 + bx + t_0$ (t is the time and x is the relative for capacity loss).

An Arrhenius behavior was found with ln K versus $1/T$ as shown in Fig. 2. The corresponding activation energy is of the order of 41.3 kJ/mol Li (0.4 eV).

3.2. The capacity losses

Fig. 3 describes the capacity loss after thermal aging at 75 °C for 10 days. After a few preliminary cycles, the discharge capacity stabilizes at the initial value of $Q_i = 135$ mAh/g. The first discharge capacity after aging falls to 40 mAh/g. The difference $135 - 40 = 95$ mAh/g is the total capacity loss Q_{tl}. Subsequent cycles show an increase in the discharge capacity, which then stabilizes at the final value of $Q_f = 100$ mAh/g. Therefore, the total capacity loss is the sum of two terms, a reversible (recoverable) one $Q_{rev} = 100 - 40 = 60$ mAh/g, and an irreversible (permanent loss) one $Q_{irr} = Q_i - Q_f = 135 - 100 = 35$ mAh/g.

Fig. 4 shows the time versus the percentage capacity loss x traces at different temperatures;

$$x\,(\%) = \frac{Q_{tl}}{Q_i} \times 100, \tag{3}$$

A fit was found with the equation:

$$t = ax^2 + bx + t_0, \tag{4}$$

Table 1
Temperature evolution of the a, b and t_0 parameters in equation $t = ax^2 + bx + t_0$ (t is the time and x is the relative for capacity loss)

T (°C)	a (h)	b (h)	t_0 (h)
60	0.144	2.305	1.226
65	0.064	2.221	3.258
70	0.0487	1.419	2.981
75	0.0376	0.840	0.523

Table 1 displays the a, b and t_0 values at different temperatures. The a parameter is equivalent to a rate constant, b relates to the initial state of the electrode and t_0 is a small time adjustment constant, which may be related to the thermal specific capacity C_p of the cell.

Fig. 5 shows the Arrhenius plot of a. A linear dependence is found, indicating the thermally activated character of the capacity loss. The associated activation energy is 81.2 kJ/mol Li, which is higher than 36.3 kJ/mol obtained in complete cells operated in the floating charge mode [3]. This difference in the activation energy may come from the operating mode itself or from contribution from the anode

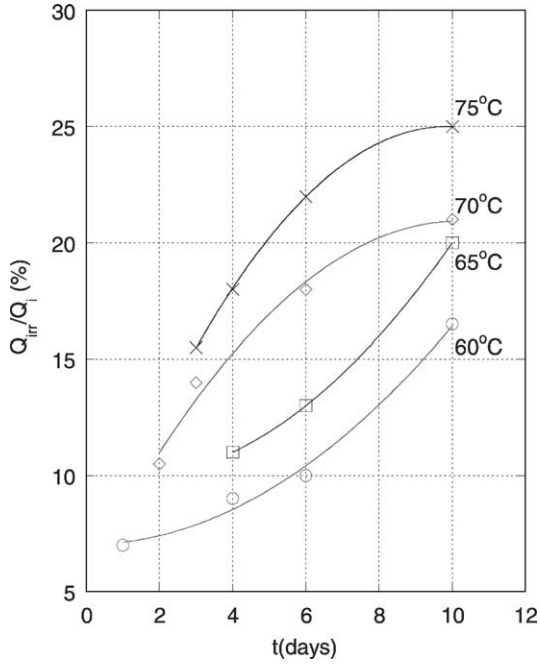

Fig. 6. Time dependence of the irreversible capacity loss at different temperatures.

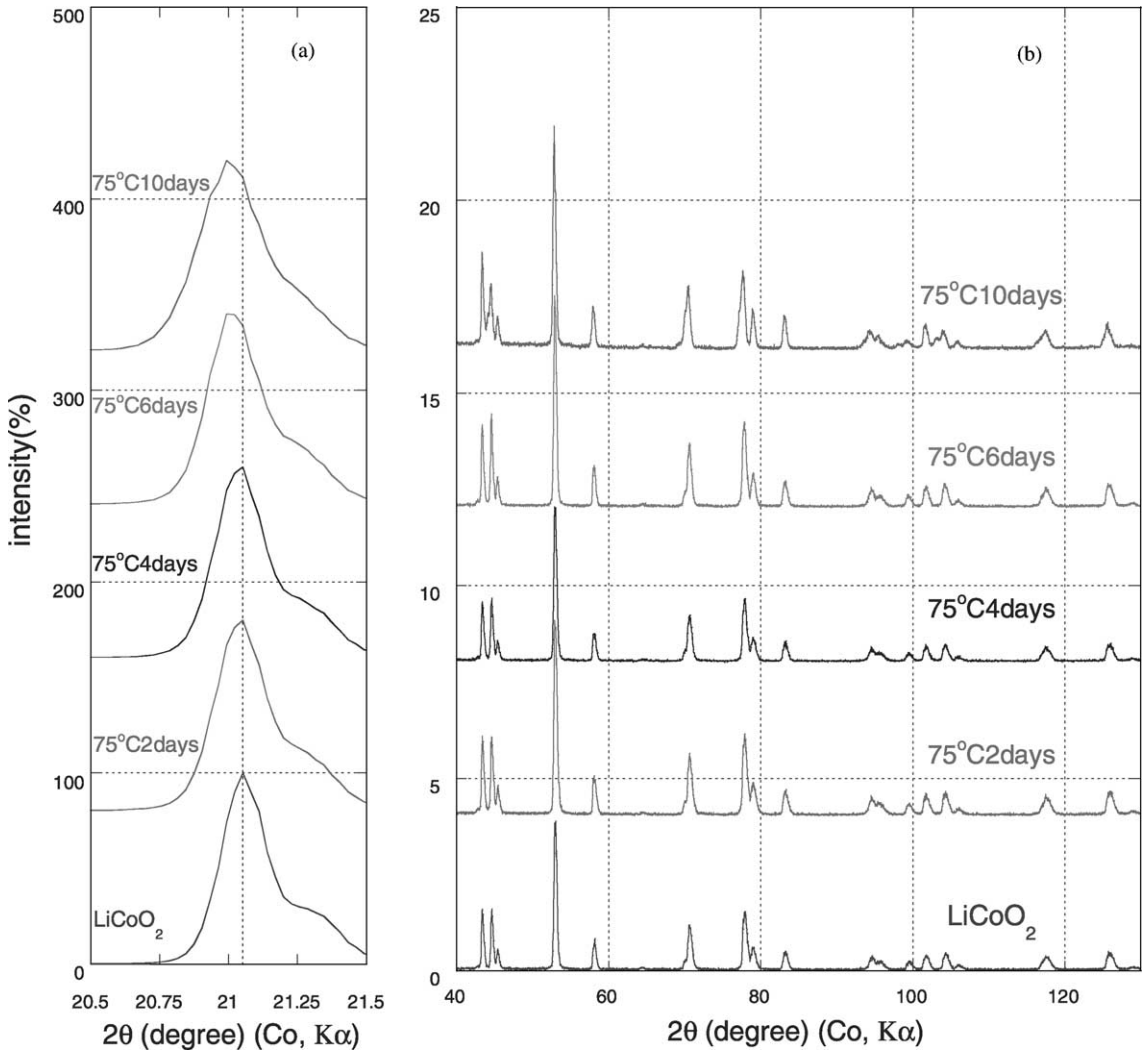

Fig. 7. XRD (Co Kα) charts of cathodes aged at 75 °C for different times. The cathodes were in their discharged state: (a) (0 0 3) peak area, (b) other peaks of lower intensities (note different intensity scales between (a) and (b)).

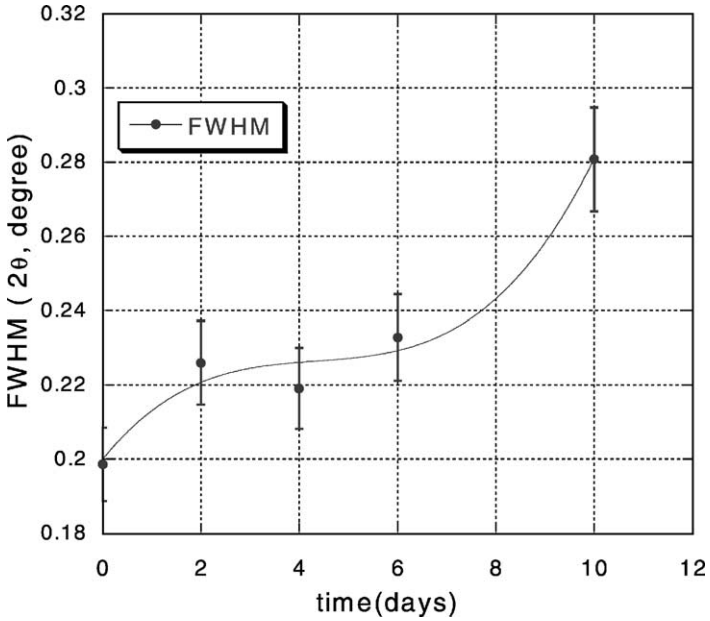

Fig. 8. Evolution of the (0 0 3) peak FWHM with aging time at 75 °C.

side, which in our case is not limiting the capacity (being in large excess unlike the study in [3]).

The time dependence of the irreversible capacity loss $Q_{irr}(t, T)$ is depicted in Fig. 6. Although as expected $Q_{irr}(t, T)$ increases monotonically with the aging time, a change in their curvature occurs between 65 and 70 °C. This may suggest a change in the mechanism controlling the irreversible capacity loss.

In order to check the crystal structure contribution to $Q_{irr}(t, T)$, XRD was performed on electrodes aged at 75 °C. Fig. 7 shows the XRD charts of samples aged between 0 (virgin) and 10 days. Samples for the XRD were in their discharge state (2.9 V). For more clarity, Fig. 7a shows the (0 0 3) strongest peak and Fig. 7b shows the rest of the pattern. All diffraction peaks appeared at almost same angular position with slightly different relative intensities. Such differences in the relative intensities could not be clearly ascribed to phase transitions since they may also result from the electrode texture, which could vary during cycling and/or aging.

The most significant change was found in the peaks broadening especially for the (0 0 3) peak. The full-width at half-maximum (FWHM) versus time curve in Fig. 8 shows an initial slow increase, followed by a steep increase after 6 days. The broadening of the (0 0 3) peak may result from internal strains within the crystallites and/or from a decrease in the coherence length along the *c*-axis. XRD can hardly distinguish between the delithiated hexagonal and the spinel phase, which may form on the grains surface. This is due to the small amounts of the spinel phase and to the fact that the two phases have similar XRD patterns. However, the broadening of the (0 0 3) peak is significant enough to assign it to modifications in the crystal structure or to decreased crystallinity of the electrode material, which may be associated with the irreversible capacity losses.

4. Conclusion

The use of $Li/Li_{1-x}CoO_2$ half-cells allowed the kinetics of the cathode contribution to the voltage decay and the capacity loss to be determined. We found empirical time dependence laws of the OCV and total capacity loss that suggest a diffusion mechanism for the former and a crystal transformation for the latter as the controlling mechanisms. Their corresponding activation energies were 41.3 and 81.2 kJ/mol Li, respectively. The crystal structure transformation resulting from increased internal strains and/or decrease in coherence length along the *c*-axis was confirmed from the (0 0 3) peak FWHM evolution upon aging.

Acknowledgements

The authors would like to thank ENAX Inc., Japan for their financial supporting and for providing $LiCoO_2$ cathode, Mitsubishi Chemicals Co., Japan and Crane Co., USA for complimentarily providing the electrolyte and the glass fiber separator, respectively.

References

[1] Y. Nishi, in: M. Wakihara, O. Yamamoto (Eds.), Lithium Ion Batteries, Fundamentals and Performance, Wiley–VCH, New York, 1998, p. 181.
[2] D. Linden, Handbook of Batteries, second ed., McGraw-Hill, New York, 1995.
[3] M. Broussely, S. Herreyre, P. Biensan, P. Kasztejna, K. Nechev, R.J. Staviewicz, J. Power Sources 97–98 (2001) 13.
[4] R. Yazami, Y.F. Reynier, Electrochim. Acta 47 (2002) 1217.
[5] H. Gabrisch, R. Yazami, B. Fultz, in: Proceedings of the 11th IMLB, Monterey, 23–28 June 2002, abstract no. 299 (and this proceedings).
[6] R.J. Gummow, M.M. Thackeray, W.I.F. David, S. Hull, Mater. Res. Bull. 27 (1992) 327.
[7] E. Rossen, J.N. Reimers, J.R. Dahn, Solid State Ionics 62 (1993) 53–60.
[8] R. Yazami, N. Lebrun, M. Molteni, M. Bonneau, J. Power Sources 54 (1995) 389.
[9] C.Y. Yao, T.H. Kao, C.H. Cheng, J.M. Chen, W.M. Hurng, J. Power Sources 54 (1995) 491.
[10] A. Honders, M.M. der Kinderen, A.H. van Heeren, J.H.W. de Wit, G.H.J. Broers, Solid State Ionics 14 (1984) 205.
[11] D.D. MacNeil, J.R. Dahn, J. Electrochem. Soc. 148 (2001) A 1205.